Int. J. Radiation Oncology Biol. Phys., Vol. 58, No. 5, pp. 1562–1569, 2004

0360-3016/04/$–see front matter

ELSEVIER

doi:10.1016/j.ijrobp.2003.12.010

BIOLOGY CONTRIBUTION

PROTON AND HYPERPOLARIZED HELIUM MAGNETIC RESONANCE IMAGING OF RADIATION-INDUCED LUNG INJURY IN RATS

ERIKA R. WARD, B.S.E.,* LAURENCE W. HEDLUND, PH.D.,† WILLIAM C. KURYLO, B.S.,† CHARLES T. WHEELER, B.S.,† GARY P. COFER, B.S.,† MARK W. DEWHIRST, D.V.M., PH.D.,* LAWRENCE B. MARKS, M.D.,* AND ZELJKO VUJASKOVIC, M.D., PH.D.*

*Department of Radiation Oncology and †Center for In Vivo Microscopy, Duke University Medical Center, Durham, NC

Purpose: To assess the usefulness of hyperpolarized helium (^{3}He) MRI, including apparent diffusion coefficient measurements, in the detection and evaluation of radiation-induced lung injury in rats.

Methods and Materials: Female Fischer-344 rats were treated to the right lung with fractionated dose of 40 Gy (5 × 8 Gy) using 4-MV photons. Conventional proton (^{1}H) and hyperpolarized (^{3}He) MRI were used to image the lungs 3–6 months after radiation treatment. Apparent diffusion coefficient (ADC) maps of hyperpolarized ^{3}He in the lungs were calculated using a nonlinear, least-squares fitting routine on a pixel-by-pixel basis. After imaging, lungs were processed for histologic assessment of damage.

Results: The effect of radiation was time dependent with progressive right lung damage ranging from mild to moderate at 3 months to severe fibrosis with structural deformation at 6 months after radiation. There was a significant decrease in the apparent diffusion coefficient of hyperpolarized ^{3}He gas in radiation-treated lungs. Areas of decreased ADC in the lungs correlated with fibrosis shown by histology.

Conclusion: This is the first study to show that hyperpolarized ^{3}He MRI can detect radiation-induced lung injury noninvasively. Reduced hyperpolarized ^{3}He ADC values postradiation likely reflect reduced alveolar volumes associated with fibrosis of the interstitium. Future studies at earlier time points may determine whether this noninvasive imaging technique can detect lung damage before clinical symptoms. Development of this new approach of magnetic resonance lung imaging in the rat model of radiation-induced lung injury will increase the ability to develop appropriate algorithms and more accurate models of the normal tissue complication probability.

Hyperpolarized gas, Helium, MRI, Radiation-induced lung damage, Helium-apparent diffusion coefficient.

INTRODUCTION

Pulmonary toxicity is a major limiting factor in thoracic radiotherapy (1–5). The lung is among the most radiosensitive organs, significantly limiting the maximum safe dose of radiation that can be delivered to treat tumors in the thorax. The currently accepted normal tissue tolerance doses have largely been derived empirically over many years, often with little supporting data. For tumors in and around the thorax, improvements in local tumor control and survival can be achieved with radiation dose escalation. This can best be accomplished with a detailed knowledge of the structural and functional factors determining radiation-induced lung tissue response. However, effective imaging of radiation-induced pulmonary injury is still inadequate. Most of the existing imaging methods are limited to structural changes with little or no ability to evaluate lung *functional* changes after irradiation (6). With a combination of structural and functional information, algorithms could be developed to predict radiation-induced lung injury and further optimize radiation treatment planning for patients with tumors in and around the thorax.

The objective of this study was to determine feasibility of *in vivo* proton (^{1}H) and hyperpolarized helium (^{3}He) gas magnetic resonance (MR) imaging for detecting and evaluating radiation-induced lung injury in rats. Helium has a high diffusion coefficient, approximately 10^5 times larger than that of water, making the potential diffusion length for alveolar gases much larger than the distal lung air spaces (7). Confining alveolar gas to smaller spaces reduces the diffusion coefficient to a degree dependent upon the size of the space (8). Therefore, measurement of the apparent diffusion coefficient of the hyperpolarized helium can be used to detect changes in the structure and function of distal gas spaces in the lungs.

It has been previously shown (7) that the apparent diffu-

Reprint requests to: Zeljko Vujaskovic, M.D., Ph.D., Department of Radiation Oncology, Box 3455, Duke University Medical Center, Durham, NC 27710. Tel: (919) 681-1675; Fax: (919) 684-8718; E-mail: vujas@radonc.duke.edu

Supported by NIH/NCRR P41 05959, NIH/NCI/SAIRP R24-CA92656, and Varian Medical Systems.

Received Aug 20, 2003, and in revised form Nov 20, 2003. Accepted for publication Dec 1, 2003.

sion coefficient (ADC) measurements of hyperpolarized ^{3}He can detect the difference in lung structure between control and emphysematous rats. Emphysema is characterized by degradation of alveolar walls and an *increase* in alveolar size, resulting in increased ^{3}He ADC values. In contrast, radiation-induced lung damage causes fibrosis and a *decrease* in alveolar size; thus we hypothesize that ^{3}He ADC values would be reduced after radiation-induced lung damage.

METHODS AND MATERIALS

Animal preparation and ventilation

Control and irradiated female Fisher-344 rats weighing between 180 and 220 g were used. Animal procedures were approved by the Duke University Institutional Animal Care and Use Committee. The irradiated rats were imaged during the 6-month interval after receiving right hemithoracic irradiation with fractionated doses (5 × 8 Gy) totaling 40 Gy (4-MV photons). For imaging, rats were first anesthetized with an injection of methohexital sodium (45 mg/kg Brevital, Eli Lilly, Indianapolis, IN) and then perorally intubated with 14-gauge, 6.1-cm intracatheter (Sherwood Medical, Tullamore, Ireland). Anesthesia was maintained with isoflurane (2.5%–3.5%) using an MRI-compatible ventilator (9). Next, a mid-line incision was made in the neck to secure ligatures around the trachea to ensure a gas-tight connection with the ventilator. The spin-exchange method, described by Middleton *et al.* (10), was used to polarize the ^{3}He. For hyperpolarized ^{3}He imaging, each breath started with a bolus of air/isoflurane (0.5 cc), then 100% ^{3}He (0.5 cc), and finally 1.0 cc of air/isoflurane. This scheme minimized the effect of oxygen depolarization of hyperpolarized ^{3}He (11) and also minimized retention of hyperpolarized ^{3}He in the lead spaces in the breathing valve and extrapulmonary airways. For proton imaging, the breathing mixture was air/isoflurane with the same tidal volumes as used for ^{3}He imaging. During imaging, the rat's heart rate, body temperature, exhaled CO_2, and airway pressure were monitored.

Imaging

A 2 Tesla 30-cm-bore magnet (Oxford Instruments, Oxford, UK) with shielded gradients (180 mT/m, GE NMR Instruments, Fremont, CA) controlled by a Signa console (General Electric Medical Systems, Milwaukee, WI) running Revision 5.5 software was used for imaging. To obtain both ^{1}H and ^{3}He images, a dual-frequency 7-cm-diameter birdcage coil was used. Frequencies of 85.5 MHz and 64.8 MHz were used for the ^{1}H and ^{3}He images, respectively. Images were acquired during a brief (400 ms) period of a breath hold after full inspiration and during 400 ms of end expiration. A radial projection sequence was used with TE = 0.9 ms, TR = 20 ms, and 20 views per breath. Each proton image required 6400 views, whereas 1600 views were used in each helium image. For the diffusion images, the sequence was modified to cycle through a series of 5 bipolar gradients from 0 to 16 Gauss/cm. Image intensity decayed as a function of $S = S_0 e^{-b(ADC)}$, S being the signal and S_0 the signal with no diffusive attenuation. The gradient factor b (which ranged from 0 to 9.4 s/cm^2) was then calculated for each image using the following equation:

$$b = \gamma^2 \left\{ \int_0^{TE} \left[\int_0^t G(t')dt' \right]^2 dt \right\} = \frac{\gamma^2 \delta^2 G^2 (4T - \delta)}{\pi^2}$$

where γ is the gyromagnetic ratio of ^{3}He (2π * 32.43E6 Hz/T), δ is the pulse duration (0.5 ms), G is the pulse amplitude, and T is the time between pulses (1 ms). To compensate for signal decay due to T_1 (T_1 = 2 h) decay, the different gradient strengths were used in a randomized order (0, 12, 4, 8, 16 G/cm, respectively).

Apparent diffusion coefficient maps were calculated on a pixel-by-pixel basis using a nonlinear least-squares fitting routine. Data analysis was accomplished using NIH ImageJ version 1.29.

Histology

After imaging, rats were killed by anesthetic overdose and the lungs fixed by endotracheal instillation and processed for conventional histology. Slices of 5 μm thickness were cut as close as possible to the corresponding planes of the MR images and then stained with hematoxylin and eosin (H&E) and Masson's trichrome.

RESULTS

In total, 25 rats, 14 of which were irradiated, were imaged for this study. Twenty successful hyperpolarized helium experiments resulted, and 11 of those rats were evaluated with apparent diffusion coefficient sequences. There was time dependent, progressive right lung damage ranging from mild to moderate at 3 months to severe fibrosis with structural deformation at 6 months after radiation. Figure 1 shows the coronal view of control lungs from the (a) ^{1}H and (b) ^{3}He with corresponding (c) H&E and (d) Masson's slices. Similar coronal images of irradiated rat lungs are shown in Fig. 2.

The ^{1}H and ^{3}He images of the irradiated right lung in Fig. 2 show evidence of lung injury by the increase (^{1}H) and decrease (^{3}He) in signal intensity. Fibrosis in these areas was confirmed in the H&E and Masson's trichrome images. Radiation-treated lungs are characterized by a thickening of alveolar walls and a decrease in alveolar size, which restricts ^{3}He diffusion, yielding a smaller ADC than normal lung. In all rats imaged, proton images of injured lungs exhibited higher signal intensities in the right lung compared to the left lung at both lung volumes. Conversely, the signal intensities in the right lung of helium diffusion images of these rats were less than those in the contralateral lung, particularly at end-expiratory volume. This suggests that the right lung had overall lower gas density than the left lung, probably related to the presence of fibrosis in the right

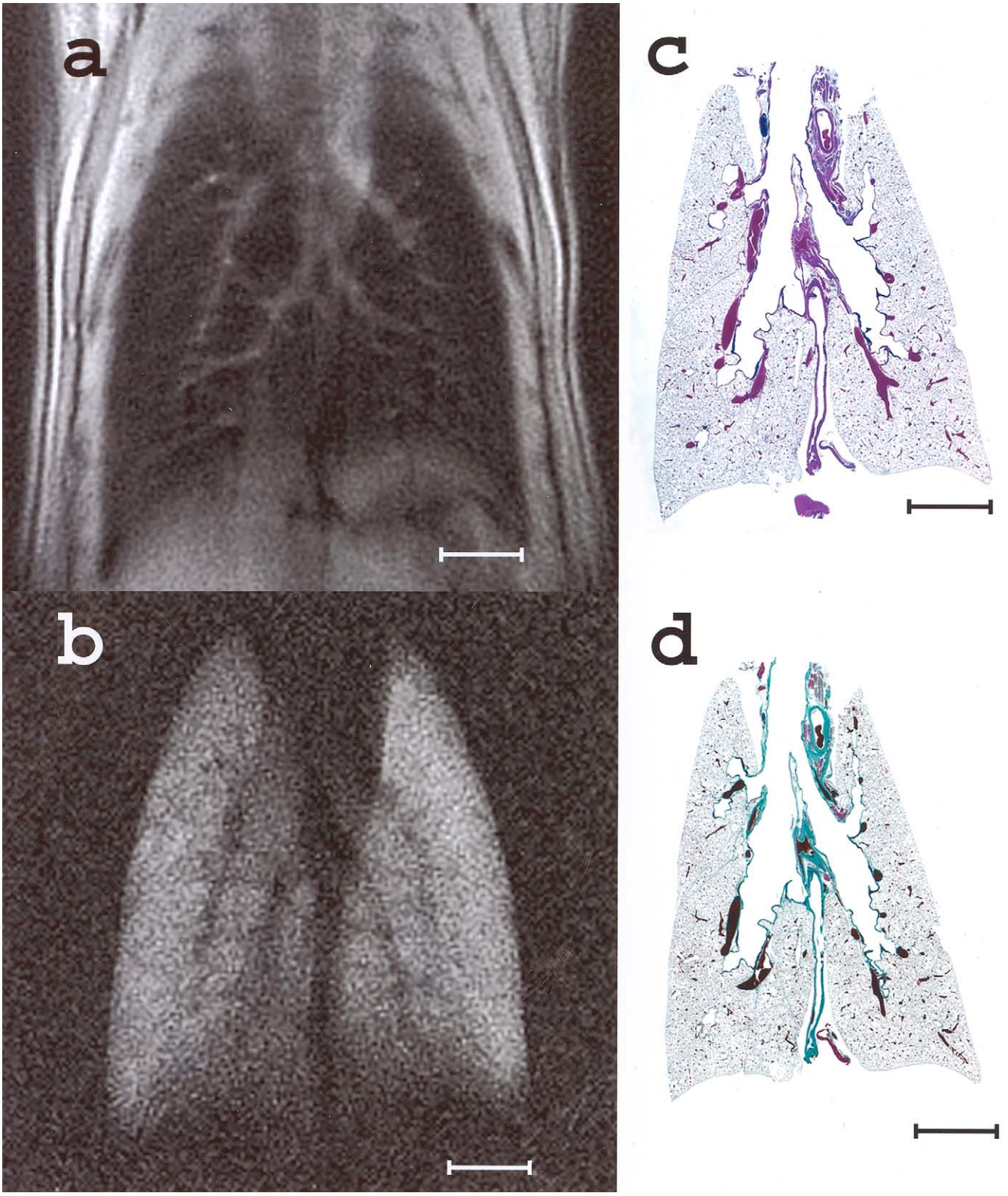

Fig. 1. Images are shown in the coronal view of both the (a) ^{1}H and (b) ^{3}He MR next to the corresponding (c) H&E and (d) Masson's trichrome slices of control rat lungs. Signal from the ^{1}H and ^{3}He images is homogeneous throughout the lung parenchyma. Lack of damage is confirmed by the healthy, nonfibrotic tissue shown in staining. Bar is equal to 5 mm.

lung (12). Figure 3 illustrates the correlation of the ^{3}He, ^{1}H images and fibrosis found in H&E images. An H&E section of an irradiated lung is superimposed on the corresponding proton image. The black and white values of the proton

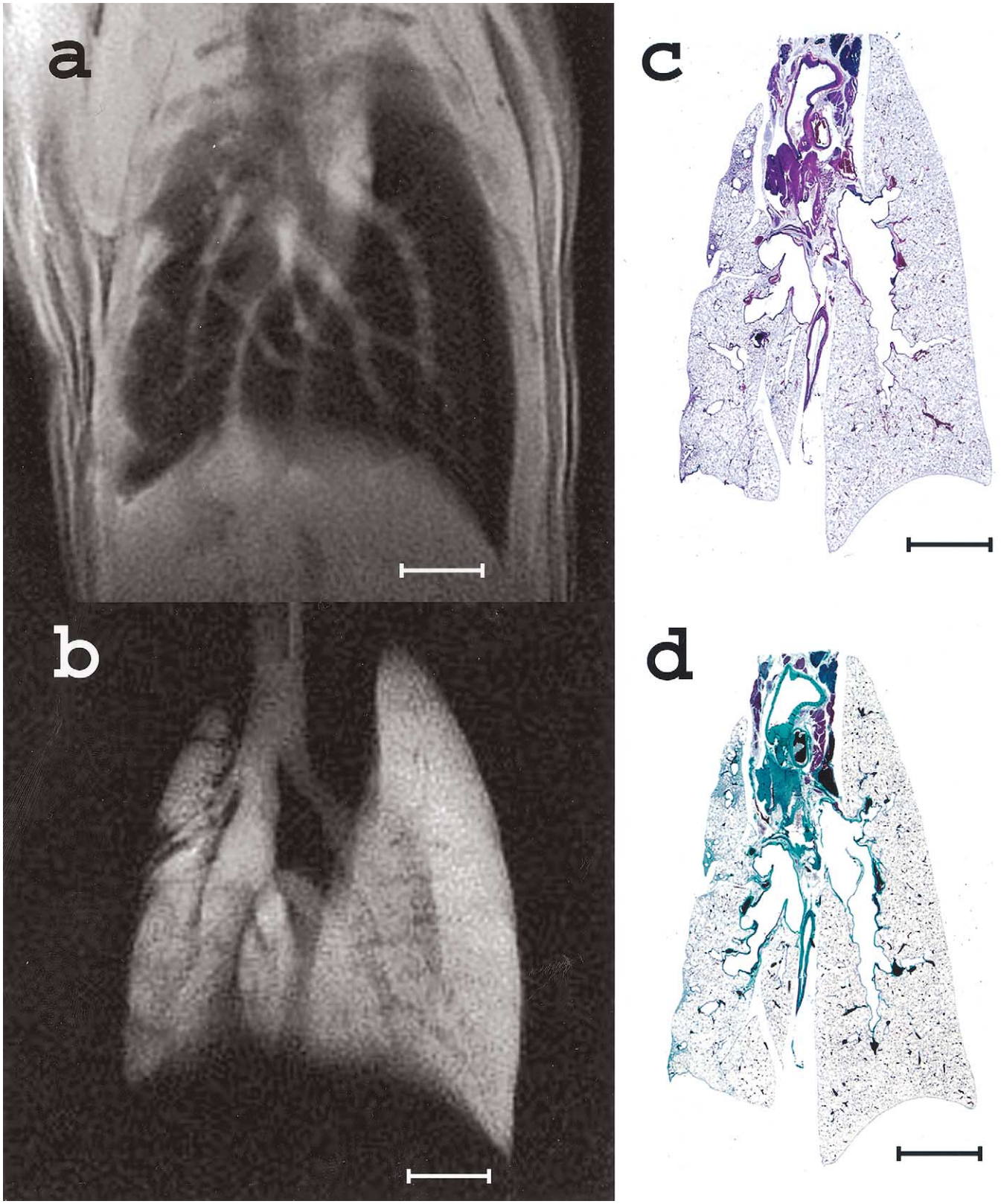

Fig. 2. Coronal images of a representative radiation-treated rat are shown 6 months after the right lung was irradiated. (a) ^{1}H, (b) ^{3}He, (c) H&E, and (d) Masson's trichrome all show significant damage to the right lung. Damage detected *in vivo* from the MR images corresponds to areas of severe fibrosis in the right lung. Bar is equal to 5 mm.

image are inverted for image clarity. Regions of interest were selected and outlined on the proton image. The signal intensities of the ^{1}H and corresponding ^{3}He image (not shown) of the regions of interest were measured and shown

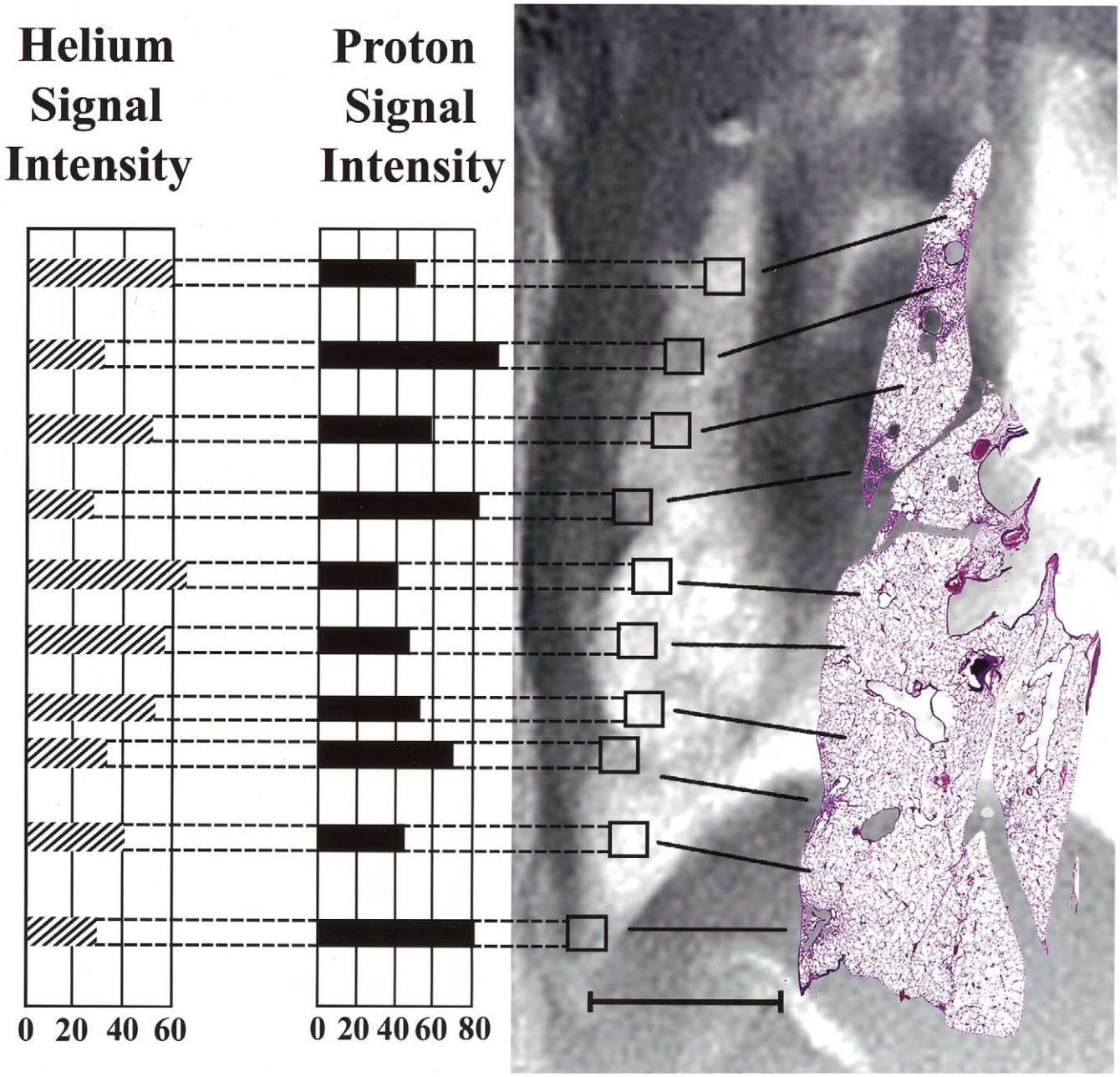

Fig. 3. ^{1}H and ^{3}He signal intensity of images in irradiated right lung as compared to histology. The H&E section is superimposed on the corresponding ^{1}H MR image. The bar graphs to the left show a measured ^{1}H and ^{3}He (image not shown) signal intensity of each outlined region of interest. A marked heterogeneity in signal from both the proton and ^{3}He images is evident in this damaged lung. Areas of fibrosis as identified in the H&E staining correspond to areas of higher signal in the ^{1}H image and lower signal in the ^{3}He image.

in the bar graphs to the left of the images. In specific regions of interest, an area of fibrosis corresponds to a low ^{3}He signal and a high ^{1}H signal. In other words, areas of fibrosis are associated with reduced gas content and increased water content.

After the ^{3}He ADC maps for both irradiated and control lungs were calculated, it was found that ADCs in the injured lungs were smaller than in the left (control) lung, suggesting that diffusion was more restricted in the irradiated right lung. Not only was the reduction in average ^{3}He ADC value of the right lung apparent, but these radiation-treated lungs exhibited a marked heterogeneity in signal. Figure 4 shows a graph of the ratios of ^{3}He ADC of the right (injured) lung over the left lung at the different times after radiation. Ratios were used instead of ADC mean values to minimize the effect of individual differences between rats. Lungs imaged between 22 and 30 weeks showed a much lower ratio than the control lungs at both end expiration ($p = 0.0003$) and held breath ($p = 0.002$). These values between control and irradiated groups were compared using Stu-

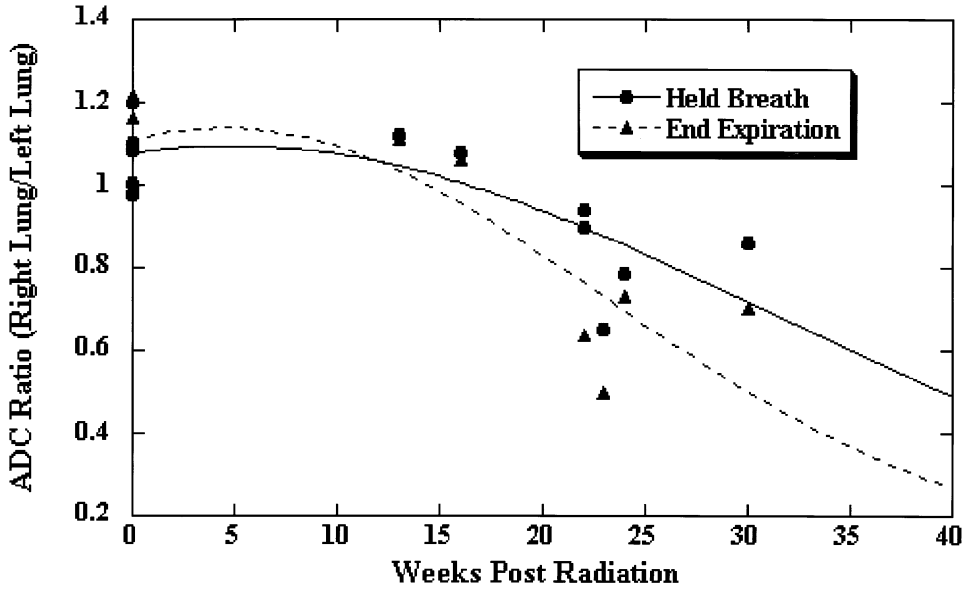

Fig. 4. Graph of ^{3}He apparent diffusion coefficient (ADC) ratio (right lung/left lung) vs. time after radiation treatment. The ^{3}He ADC value of the right lung consistently decreases relative to the left lung with increasing time after radiation. A ratio of average ADC of right to left lung is used to help cancel out individual differences between animals. The solid (held breath) and dashed (end expiration) lines represent a fit of the data to the linear-quadratic equation $y = a + \exp(-bx - cx^2)$.

dent's *t* test, in which a *p* value of less than 0.05 indicates statistical significance of difference between groups. Both proton and helium images in the radiated rats exhibited compensatory hyperinflation of the left lung, as evidenced by increased left lung field areas in axial images.

Figure 5 shows histograms derived from ^{3}He ADC maps of distal air spaces in representative control and radiation treated rats. In the untreated rat, the ADC values of the left and right lungs show no appreciable difference. This holds true for both held-breath and end-expiration volumes. In contrast, the left-to-right mean ADC values in the radiation-treated rats (24 weeks post radiation) show significant differences. At both volumes, the irradiated right lung shows a shift to lower average ADC values. At end expiration, the right lung has a mean ADC of 0.162 cm^2/s, lower than the left lung average of 0.222 cm^2/s. Similarly, at held breath, the right lung, with a mean ADC of 0.286 cm^2/s, is considerably less than the left lung, with a mean of 0.365 cm^2/s. Also to be noted is the reduced volume of the right lung in the irradiated rat, as indicated by the smaller number of points on the histogram.

DISCUSSION

The objective of this research study was to examine radiation-induced lung injury using hyperpolarized helium MRI as a tool, along with existing imaging techniques. Existing lung imaging methods, such as ^{1}H MRI and CT scanning image only lung structure. Conversely, hyperpolarized ^{3}He MRI provides both functional (gas distribution) and structural information. Conventional ^{1}H, as well as hyperpolarized ^{3}He MRI, have been used to assess pulmonary damage caused by emphysema in humans and animals, but this is the first study in which hyperpolarized ^{3}He MRI and measurement of helium ADC have been used to detect radiation-induced lung injury.

The ^{3}He images produced in this study provided a visual indicator of which areas of the lung were inflated and functional, information not apparent from the corresponding ^{1}H images. Our results from the diffusion calculations were encouraging and confirmed our predictions about the relationship between ^{3}He ADC value and lung damage, i.e., that a decrease in ADC indicates an area of fibrosis. An estimated degree of functionality can be determined from the calculated ADC maps, because the value is directly related to restriction in the movement of gas. Results from our study show that *in vivo* measurement of ^{3}He ADC correlates with known structural changes in the lung caused by radiation-induced lung injury. Therefore, we have shown this method to be a sensitive indicator of altered lung microstructure.

Using only ^{1}H MR to image lungs has proved difficult and sometimes ineffective. Proton MR signal intensity in the lung is weak due to low proton density and therefore difficult to use in damage assessment (13). Newcomb *et al.* (14) attempted to assess radiation-induced lung damage of excised rat lungs using T_1 and T_2 relaxation times measured at different time periods after irradiation. T_2 relaxation times of the radiation-damaged lungs showed a 10% increase. However, this was deemed too small an increase to affect image contrast. In our own study with proton images, the signal increase in damaged lungs provided some information as to the changes in lung structure that were confirmed by histology. However, ^{1}H images could not quantitatively

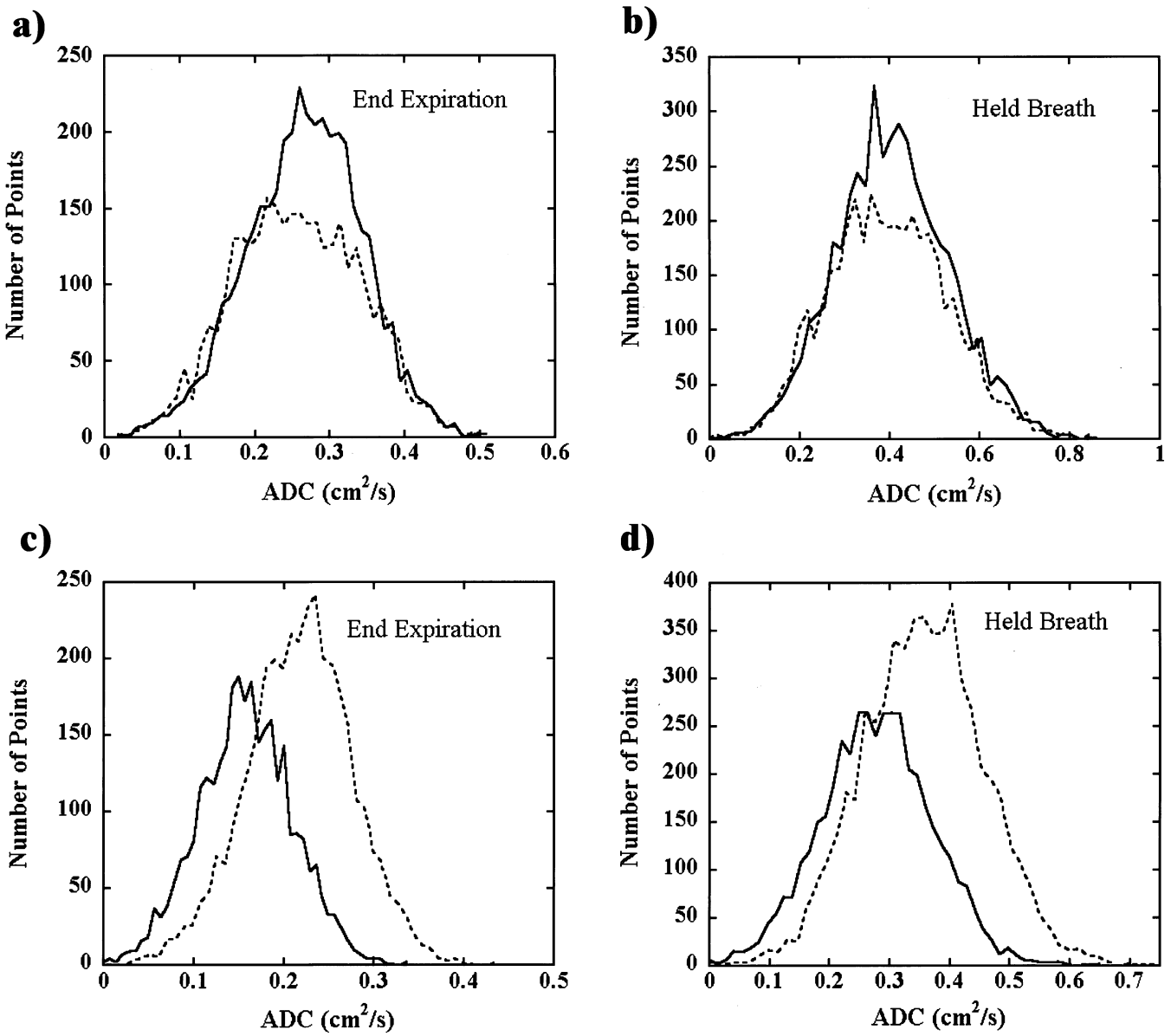

Fig. 5. Histograms of ^{3}He apparent diffusion coefficients (ADCs) are shown in a representative (a, b) control and (c, d) radiation-treated rat. ADC values of right lung (solid line) and left lung (dashed line) are compared at both end expiratory volume and held breath. Control lungs show no difference in ADC values between right and left lungs. However, at both volumes in the radiation-treated rat, right lung shows a lower average ADC. At end expiration, the right lung has a mean ADC of 0.162 cm^2/s, lower than the left lung average of 0.222 cm^2/s. Similarly, at held breath, the right lung, with a mean ADC of 0.286 cm^2/s is considerably less than the left lung, with a mean of 0.365 cm^2/s.

assess change in lung function. Short T_2 and T_2* echo times, because of the large number of gas–water interfaces, have also been a limiting factor in conventional MRI (15). However, techniques such as multislice gradient echo sequencing (16) and projection-reconstruction (15) have greatly improved image quality and signal intensity. Combining these techniques with ^{3}He ADC measurements could provide both qualitative and quantitative information about lung structure and function.

Several studies have been done with hyperpolarized ^{3}He MRI to detect changes in the lung due to diseases such as asthma (13), cystic fibrosis, emphysema (17), and chronic obstructive pulmonary disease (18, 19). Saam *et al.* (17) conducted a study comparing the ^{3}He diffusion in lungs of emphysematic patients with that in normal subjects. Histograms of ^{3}He ADCs in the lungs of patients with severe emphysema showed a wider range with larger mean values compared to those for control patients. Hyperpolarized helium MRI was also used to image lungs of asthmatic human subjects (13). Ventilation defects were identified in the ^{3}He images of asthmatic subjects that were not found in control subjects. The success of ^{3}He MRI in a clinical setting is encouraging for the future of our research and for the possibility of detecting radiation-induced lung damage in humans.

Chen *et al.* (7) studied emphysematous (elastase induced) vs. normal lungs using the apparent diffusion coefficient of hyperpolarized ^{3}He *in vivo* in the rat model. This study showed that the ^{3}He ADC of emphysematous lungs was significantly higher, even though the rats were clinically asymptomatic. H&E sections confirmed that the injured areas with a higher ^{3}He ADC were found to have enlarged distal air spaces, caused by degradation of alveolar walls, compared to control sections. Similarly, our findings indicate that lung areas with more fibrosis, thicker alveolar walls, and smaller air spaces had much lower ^{3}He ADC values. These relationships are encouraging, because they suggest that in addition to identifying lung injury, diffusion measurements can help distinguish between *types* of lung injury.

In conclusion, this is the first study to show that hyperpolarized ^{3}He imaging is a useful tool for studying radiation-induced lung injury noninvasively. ADC measurements, in particular, provide a quantitative assessment of lung function that has not previously been available. These *in vivo* measurements are a sensitive predictor of structural and functional lung changes that occur after thoracic radiation treatment.

Future studies at early time points should determine whether this noninvasive imaging technique could detect lung damage before onset of respiratory complications. Longitudinal studies may also be beneficial in studying the time course of lung injury over a period of months. Development of this new approach of MR lung imaging in the rat model of radiation-induced lung injury will increase our ability to develop appropriate algorithms and more accurate models of normal-tissue complication probabilities.

REFERENCES

1. Abratt RP, Morgan GW. Lung toxicity following chest irradiation in patients with lung cancer. *Lung Cancer* 2002;35: 103–109.
2. Lingos TI, Recht A, Vicini F. Radiation pneumonitis in breast cancer patients treated with conservative surgery and radiation therapy. *Int J Radiat Oncol Biol Phys* 1991;21:355–360.
3. Martel MK, Ten Haken RK, Hazuka MB, *et al.* Dose-volume histogram and 3-D treatment planning evaluation of patients with pneumonitis. *Int J Radiat Oncol Biol Phys* 1994;28:575–581.
4. Roach M, Gandara DR, You HS, *et al.* Radiation pneumonitis following combined modality therapy for lung cancer: Analysis of prognostic factors. *J Clin Oncol* 1995;13:2606–2612.
5. Rothwell RI, Kelly SA, Joslin CA. Radiation pneumonitis in patients treated for breast cancer. *Radiother Oncol* 1985;4:9–14.
6. Park KJ, Chung JY, Chun MS, *et al.* Radiation-induced lung disease and the impact of radiation methods on imaging features. *Radiographics* 2000;20:83–98.
7. Chen XJ, Hedlund LW, Möller HE, *et al.* Detection of emphysema in rat lungs by using magnetic resonance measurements of ^{3}He diffusion. *PNAS* 2000;97:11478–11481.
8. Salerno M, Altes TA, Mugler JP, *et al.* Hyperpolarized noble gas MR imaging of the lung: Potential clinical applications. *Eur J Radiol* 2001;40:33–44.
9. Hedlund LW, Johnson GA. Mechanical ventilation for imaging the small animal lung. *ILAR J* 2002;43:159–174.
10. Middleton H, Black R, Saam BT, *et al.* MR-imaging with hyperpolarized He-3 gas. *Magn Reson Med* 1995;33:271–275.
11. Hedlund LW, Möller HE, Chen XJ, *et al.* Mixing oxygen with hyperpolarized ^{3}He for small-animal lung studies. *NMR Biomed* 2000;13:202–206.
12. Vujaskovic Z, Batinic-Haberle I, Rabbani ZN, *et al.* A small molecular weight catalytic metalloporphyrin antioxidant with superoxide dismutase (SOD) mimetic properties protects lungs from radiation-induced injury. *Free Radic Biol Med* 2002;33:857–863.
13. Altes TA, Powers PL, Knight-Scott J, *et al.* Hyperpolarized ^{3}He MR lung ventilation imaging in asthmatics: Preliminary findings. *J Magn Reson Imaging* 2001;13:378–384.
14. Newcomb CH, Van Dyk J, Hill RP. The role of magnetic resonance for assessing radiation-induced lung damage. *Int J Radiat Oncol Biol Phys* 1994;30:125–132.
15. Gold GE, Pauly JM, Leung AN, *et al.* Short echo time MR spectroscopic imaging of the lung parenchyma. *J Magn Reson Imaging* 2002;15:679–684.
16. Beckmann N, Tigani B, Mazzoni L, *et al.* MRI of lung parenchyma in rats and mice using a gradient echo sequence. *NMR Biomed* 2001;14:297–306.
17. Saam BT, Yablonskiy DA, Kodibagkar VD, *et al.* MR imaging of diffusion of He-3 gas in healthy and diseased lungs. *Magn Reson Med* 2000;44:174–179.
18. de Lange EE, Mugler JP, Brookeman JR, *et al.* Lung air spaces: MR imaging evaluation with hyperpolarized He-3 gas. *Radiology* 1999;210:851–857.
19. Kauczor HU, Ebert M, Kreitner KF, *et al.* Imaging of the lungs using 3He MRI: Preliminary clinical experience in 18 patients with and without lung disease. *J Magn Reson Imaging* 1997;7:538–543.